Communications

Digital Ray Tracing for Geotomography

Andrew G. Tallin and J. Carlos Santamarina

I. INTRODUCTION

Tomographic methods have been used in a number of disciplines for the last decade, including medicine, material science, and geophysical research. Tomographic imaging of an unknown region is based on external measurements of media-sensitive parameters. Each measurement is a line integral of the form,

$$y = \int_a^b p(x(s))ds \tag{1}$$

where $x(s)$ is the parametric equation of an arc from a to b, and $p(.)$ is some position-dependent function usually called the picture function. For geotechnical applications when a mechanical wave is used, the function $p(.)$ is the wave slowness and the measurement y is the travel time from the source a to the sensor b.

Given a large enough set of independent measurements, it is possible to estimate the picture function. This process is usually called reconstruction. In medical applications (e.g., CAT scans) measurements can be made around $360°$ and the reconstruction methods take advantage of the axial symmetry of the measurements. This is not possible in many applications such as geotechnical site investigation. In this case, the region to be imaged is discretized into a rectangular grid of cells and the picture function becomes a vector of cell values, p. Then, (1) is approximated with a summation, and the measurements y are written as a function of the cell values p as,

$$y = Rp \tag{2}$$

The element r_{ij} in the R matrix represents the transit length of the ith arc over the jth cell (see Fig. 1(a)). There are a number of methods to estimate the best vector p that satisfies (2) based on the measurement set y. Because of the large size of the R matrix, iterative solutions are preferred over the direct solution of the least square problem [2], [3].

The determination of the r_{ij} coefficients is often the most time consuming step in reconstructing the image. For example, when an iterative method is used to do the reconstruction, the cpu time spent in calculating the coefficients in R is often more than ten times the time spent in each iteration. In straight ray tomography R is calculated only once. However, most algorithms that take into consideration ray bending require frequent reevaluation of R and the time required to calculate it has a major effect on the efficiency of the algorithm. This paper examines two methods of determining the coefficients in R. Straight rays have been assumed to facilitate the presentation.

II. EXACT SOLUTION: PARAMETRIC EQUATION

This first method calculates the exact distance traveled by the ith ray over the jth cell, r_{ij}. In this case, the most direct way to compute

the r_{ij} coefficients is based on the parametric form of the line that represents the ray traveling from the source at location (x_0, y_0) and the receiver at location (x_1, y_1),

$$x = x_0 + s(x_1 - x_0) \tag{3a}$$
$$y = y_0 + s(y_1 - y_0) \tag{3b}$$

where s is a line coordinate which varies from 0 at the source to 1 at the receiver.

The ith row in R contains the transit lengths of the ith ray in the different cells. The algorithm to compute the nonzero r_{ij} components of R proceeds as follows:

1) Calculate, in terms of s, the boundary–ray intersections. Consider all horizontal cell boundaries between y_0 and y_1 and all vertical cell boundaries between x_0 and x_1.

2) Save all s values in a list. Add to this list the line coordinates of the source and receiver, $s = 0$ and $s = 1$. Sort the list in increasing order of s and eliminate repeated values of s (this takes place when the ray intersects two convergent cell boundaries at the corner). The resulting list is:

$$S = \{0, s_1, s_2, \ldots s_n, 1\} \tag{4}$$

3) Two adjacent values in the list S, s_t and s_{t+1} correspond to the same cell which can be identified by selecting the cell that contains a point on the ray with line coordinates s lying between s_t and s_{t+1}. The difference $(s_{t+1} - s_t)$ is the fraction of the ray length across the cell. The product of the difference and the total ray length is the coefficient in R with a row index corresponding to the ray and a column index corresponding to the cell.

The algorithm has been implemented using dynamic linked list structures in order to facilitate development, sorting and storage of both the list S and the rows in R (see, e.g., [1]). Compound data structures, in which the cell index is bound with the element values, are used to store only the nonzero row elements of R.

III. APPROXIMATE SOLUTION: DIGITAL RAY TRACING

The iterative nature of the reconstruction algorithm, noise in the measurements, and hardware limitations may not warrant high accuracy in the determination of r_{ij} coefficients. In the extreme case, only a 0 or 1 indication of whether a cell is touched by a ray could be required [2]. The digital ray tracing presented next evolves from this concept, and is related to Bresenham's algorithm, often used for drawing lines in pixel-based graphic display hardware.

The method begins by subdividing the region to be imaged into cells. Each cell is represented by a rectangular array of pixels. The granularity of the pixel grid is the number of pixels per cell k^2, where k is the number of pixels to the side of a cell. In this new representation, a ray has only integer pixel coordinates (Fig. 1(b)), stretching between (u_0, v_0) and (u_1, v_1). Then, the ray is approximated by a stair case of pixels. The coefficient r_{ij} is obtained as the ratio between the number of pixels in the jth cell touched by the ith ray, and the total number of pixels that form the ith ray.

For a ray with positive slope, and traced from left to right, the "next" pixel is one of the following three: the one above, the one to the right, or the one diagonally to the right and above the current
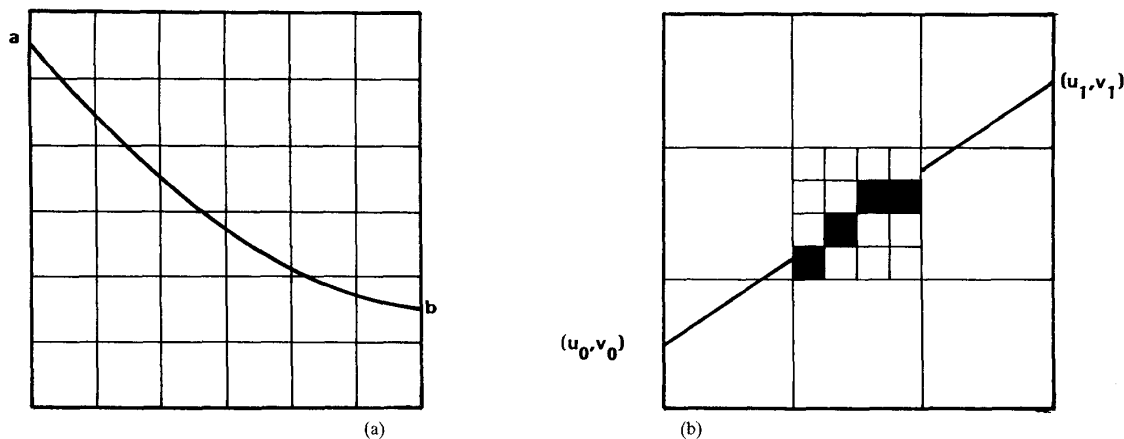
Fig. 1. Exact and approximate solution—schematic representation.

position. The chosen "next" pixel is the one that minimizes the difference between the real line and its stair case representation. If the pixel's relative position to the source is denoted by (u, v) and the total offset between the source and the receiver by $(U, V) = (u_1 - u_0, v_1 - v_0)$, the difference between the stair case and the line can be defined in terms of the difference between the ratio u/v and the ratio U/V. This can be rearranged to form the residual,

$$res = u \times V - v \times U \tag{5}$$

Because pixel coordinates are integers, the expression for the residual at the "next" pixel, res_{k+1} can be obtained iteratively, from the current value, res_k: (1) If the next pixel is above the present position, then v is increased by one and $res_{k+1} = res_k - U$; (2) if the next pixel is to the right $res_{k+1} = res_k + V$; and (3) if the next pixel is above and to the right $res_{k+1} = res_k + V - U$. Similar expressions are obtained in the case of a negatively sloping ray. The algorithm is simple, and begins at (u_0, v_0). The slope of the ray is checked and the corresponding three expressions for the residual are computed. The pixel with the smallest residual is selected or "lit," and its residual becomes the current value of the residual. Then, the algorithm is repeated from this new pixel.

Extension to the calculation of the r_{ij} coefficients to nonstraight rays requires the residuals to be calculated based on the local values of the curve at each of the neighboring pixels, in order to choose the next pixel to be lit. Unless the form of the equation of the curve is simple this would require a substantial amount of calculation. On the other hand, the length of the ray can be simply determined from the number of lit pixels.

IV. COMPARISON

The two algorithms were implemented in arttool, which run under the SunView windowing system on a Sun-3 workstation [4], [5]. (arttool, includes ART, SIRT, and CR algorithms to perform the reconstruction). The performance of the two R generation algorithms were compared by measuring the time required to develop R. Three levels of resolution were considered within the range relevant to geotechnical tomography: 8×8, 16×16 and 32×32 cells per image. Granularity varied from 1 to 20^2 pixels per cell. Fig. 2 presents a plot of measured ray processing times as a function of the pixel granularity in each case.

Several observations concerning the quality of the image and the speed of the algorithm can be made. The time required to generate R by the digital method is approximately linear with the granularity.
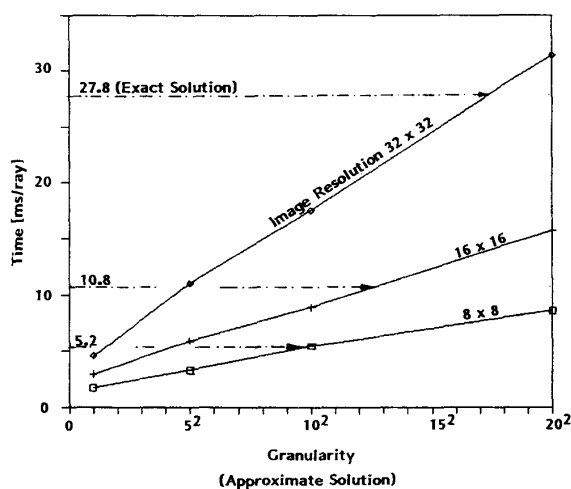
Fig. 2. Exact and approximate solution — comparison.

The performance of the exact method decreases more rapidly as a function of the number of cells (image discretization) than does the digital method. The performance of the digital method for a region discretized to a 8×8 grid and granularity of 10^2 are approximately the same as the exact, while the performance of the digital method applied to a 32×32 cell grid and a granularity of 17^2 is approximately the same as the exact method.

As the image discretization increases the effect of inaccuracies in the digital approximation decreases. For example, there was no difference observed between the images obtained with the exact method and the digital method with a granularity of 5^2, when the image discretization is 32×32. In general, the images produced with granularities of about 5^2 are as good as those obtained from the exact R. This observation highlights the advantage of the approximate method when applied to finer grids.

Similar findings were obtained using the conjugate gradient reconstruction method (CR) and are summarized in Table I. For this analysis synthetic data for a hypothetical stratigraphy was reconstructed in a 16×16 cell image.

Finally, because the digital method can be implemented using only integer arithmetic, its relative performance over the exact

TABLE I
CR RECONSTRUCTION

Granularity	Error	Image
1	0.01419	unrecognizable
5	1.09×10^{-5}	acceptable
10	6.347×10^{-5}	good
20	8.993×10^{-6}	good

method should be even better on hardware that does not depend on software to perform floating point operations (e.g., PC without a math coprocessor).

REFERENCES

[1] P. C. Brillinger and D. J. Cohen, *Introduction to Data Structures and Non-Numeric Computation.* Englewood Cliffs, NJ: Prentice-Hall, 1972.

[2] K. A. Dines and R. J. Lytle, "Computerized geophysical tomography," *Proc. IEEE,* vol. 67, no. 7., 1979.

[3] S. Ivansson, "Seismic Borehole Tomography—theory and computational methods," *Proc. IEEE,* vol. 74, no. 2, pp. 328–338, 1986.

[4] A. G. Tallin and J. C. Santamarina, "Geotomographic site investigation software," presented at the Proc. of the 7th National Conference on Microcomputers in C. E., Orlando, FL, 1989.

[5] A. G. Tallin and J. C. Santamarina, "Geotomography in site investigation—simulation study," *Geotechnical Testing Journal,* ASTM, June 1990.

Effect of Wind on FM-CW Radar Backscatter from a Wet Snowcover

Gary Koh

Abstract—The most important factor affecting the microwave properties of a snowcover is the liquid water content (snow wetness). An FM-CW (26.5–40 GHz) radar has been used to investigate the influence of snow wetness on the magnitude of radar backscatter from a snowcover. The radar backscatter measurements from a wet snowcover on a windy day suggest that evaporative cooling due to the wind may reduce the amount of liquid water at the snowcover surface.

I. INTRODUCTION

The study of microwave interaction with a snowcover is important for radar remote sensing applications in a winter environment. Previous studies on the relationship between the physical and microwave properties of a snowcover have shown that the presence of liquid water (snow wetness) is the most important factor that can affect the performance of a microwave radar [1]–[7]. Due to the large difference in the complex dielectric constants of ice and water in the microwave regions, the presence of even a small amount of liquid water can affect the magnitude of the radar backscatter from a snowcover. An example of this phenomenon is the diurnal variation of radar backscatter as a snowcover undergoes gradual melting and freezing cycles [1],[3].
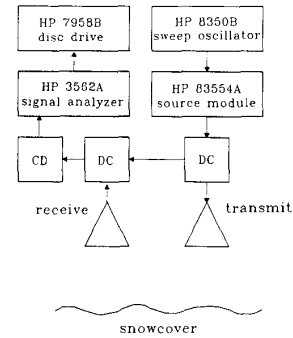
Fig. 1. Schematic of the FM-CW radar used to measure backscatter from a snowcover. DC and CD are directional coupler and crystal detector.

Because of the importance of the liquid water on the microwave properties of a snowcover, the conditions that can lead to an increase or decrease in the snow wetness are of interest. The air temperature and the incoming solar radiation are obvious indicators of snow wetness. The influence of wind on snow wetness and the resulting effect on radar backscatter are perhaps less obvious. Measurements of FM-CW (26.5–40 GHz) radar backscatter from a snowcover during a windy day suggest that evaporative cooling due to the wind may reduce the amount of liquid water at the snowcover surface. These results were observed during a study that was recently initiated to investigate the dynamics of a snowcover using an FM-CW radar.

II. EXPERIMENT

The FM-CW radar system used in this study is illustrated in Fig. 1. An HP8350B sweep oscillator and an HP83554A millimeter-wave source module generate signals whose frequency varies linearly with time from 26.5 to 40 GHz with a sweep time of 80 ms. A directional coupler divides the frequency-modulated signals into two paths; a reference signal is brought directly into a mixer (directional coupler and crystal detector) and a target signal is routed to the snowcover via a transmitting horn lens antenna. The reflected signal from the snowcover is fed into the mixer input via a receiving antenna. An HP3562A signal analyzer is used to obtain the fast Fourier transform (FFT) of the mixer output and an HP7958B disc drive is used to store the FFT's. The FFT of the mixer output yields a spectrum whose frequency is proportional to the target distance and whose amplitude is proportional to the target reflectivity. The FM-CW radar described above is sensitive to change in the dielectric properties of the target down to the scale length of approximately $\frac{2.0}{\sqrt{\epsilon}}$ cm, where ϵ is the effective dielectric constant of the target.

The FM-CW radar is mounted on a gantry approximately 6.0 m above the snowpack and positioned so that the transmitted signal is directed toward the snowcover at a $4°$ incident angle. The radar is stationary so that the backscatter from the same spot on the snowcover is always measured. The backscatter data were initially collected by visually monitoring the real time display of the FFT's. The data acquisition process is now automated and the radar backscatter measurements are made once every 10 min. The air temperature and wind speed are recorded with an instrumented tower located approximately 30 m from the radar. The incoming solar radiation is recorded with an Epply pyranometer.